ACS Photonics

pubs.acs.org/journal/apchd5

Article

Tunable Cavity Coupling to Spin Defects in a 4H-Silicon-Carbide-On-Insulator Platform

Tongyuan Bao, Qi Luo, Ailun Yi, Bo Liang, Yao Zhang, Hai-Bo Hu, Shen Lai, Zhengtong Liu, Shumin Xiao, Xin Ou,* Yu Zhou,* and Qinghai Song*

Cite This: *ACS Photonics* 2025, 12, 2988−2996

Read Online

ACCESS | Metrics & More | Article Recommendations | Supporting Information

ABSTRACT: Silicon carbide (SiC) has attracted significant attention as a promising quantum material due to its ability to host long-lived, optically addressable color centers with solid-state photonic interfaces. The CMOS compatibility of 4H-SiCOI (silicon-carbide-on-insulator) makes it an ideal platform for integrated quantum photonic devices and circuits. While microring cavities have been extensively studied in SiC and other materials, the integration of 4H-SiC spin defects into these critical structures, along with continuous mode tunability, remains unexplored. In this work, we demonstrate the integration of PL4 divacancy spin defects into tunable microring cavities in scalable thin-film 4H-SiC nanophotonics. Comparing on- and off-resonance conditions, we observed an enhancement of the Purcell factor by approximately 5.0. This enhancement effectively confined coherent photons within the coupled waveguide, leading to a 2-fold increase in the ODMR (optically detected magnetic resonance) contrast and coherent control of PL4 spins. These advancements lay the foundation for developing SiC-based quantum photonic circuits.

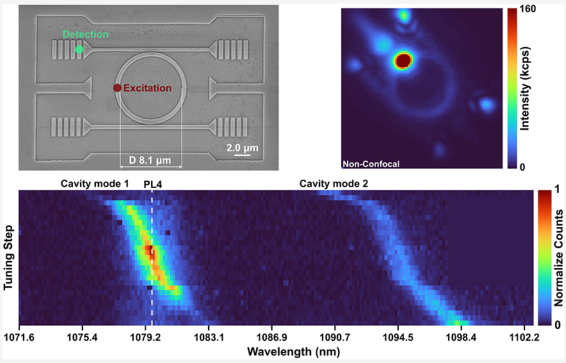

KEYWORDS: *silicon carbide, quantum photonic devices, spin defects*

INTRODUCTION

Long-lived and optically addressable spin defects in silicon carbide[1,2] are emerging as a promising quantum candidate due to their robustness, versatile control,[3−6] and developed read-out methods.[7,8] One advantage of silicon carbide compared to diamond is its compatibility with complementary metal-oxide-semiconductor (CMOS) fabrication technology.[9,10] This makes 4H-SiCOI (silicon-carbide-on-insulator) a promising platform for advancing integrated quantum photonic devices and circuits.[9−13] However, leveraging 4H-SiCOI for the continued scaling up quantum networks presents a significant challenge: achieving precise and continuous tunability of the interaction between photonic cavities and spin defects.[12,14−17] This is especially important for enhancing zero-phonon line (ZPL) emissions over those in the phonon sideband. Boosting emissions into the ZPL is essential for achieving key milestones in the construction of quantum networks, such as single-shot readout,[1,7,18] spin-photon entanglement,[19,20] and heralded between remote nodes,[21−23] where coherent and indistinguishable photons are needed.

Cavity-coupled color centers have been demonstrated using 4H-SiC 1D nanobeam cavities created through bulk carving techniques,[14,15,24] and 3C-SiC 2D photonic cavities.[25] Advances in quantum-grade 4H-SiCOI thin films[12] have opened new opportunities for photonic integration. For instance, suspended 4H-SiC-on-insulator (SiCOI) microdisk resonators coupled to V_{Si} color centers demonstrate progress in this material via undercut techniques.[26] The microring cavity, a key element in nonlinear optics and photonics,[27,28] offers several advantages: its in-plane geometry allows seamless coupling to waveguides through evanescent fields, enabling low-loss on-chip photon routing and modular interconnects for scalable architectures. Its nonsuspended structure ensures mechanical stability during fabrication. Notably, the CMOS-compatible fabrication process allows for wafer-scale integration with established photonic platforms, reducing costs and complexity for mass production. While microring cavities have been fabricated in SiC[12,29] and other materials,[30,31] the integration of 4H-SiC spin defects into this critical structure, along with continuous mode tunability, has not yet been achieved. In this work, we address this gap by demonstrating the monolithic integration of PL4 divacancy spins into tunable microring resonators on thin-film 4H-SiC, laying the groundwork for developing SiC-based quantum photonic circuits.

Received: December 23, 2024
Revised: April 15, 2025
Accepted: April 15, 2025
Published: April 22, 2025

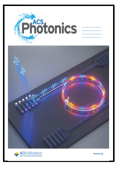

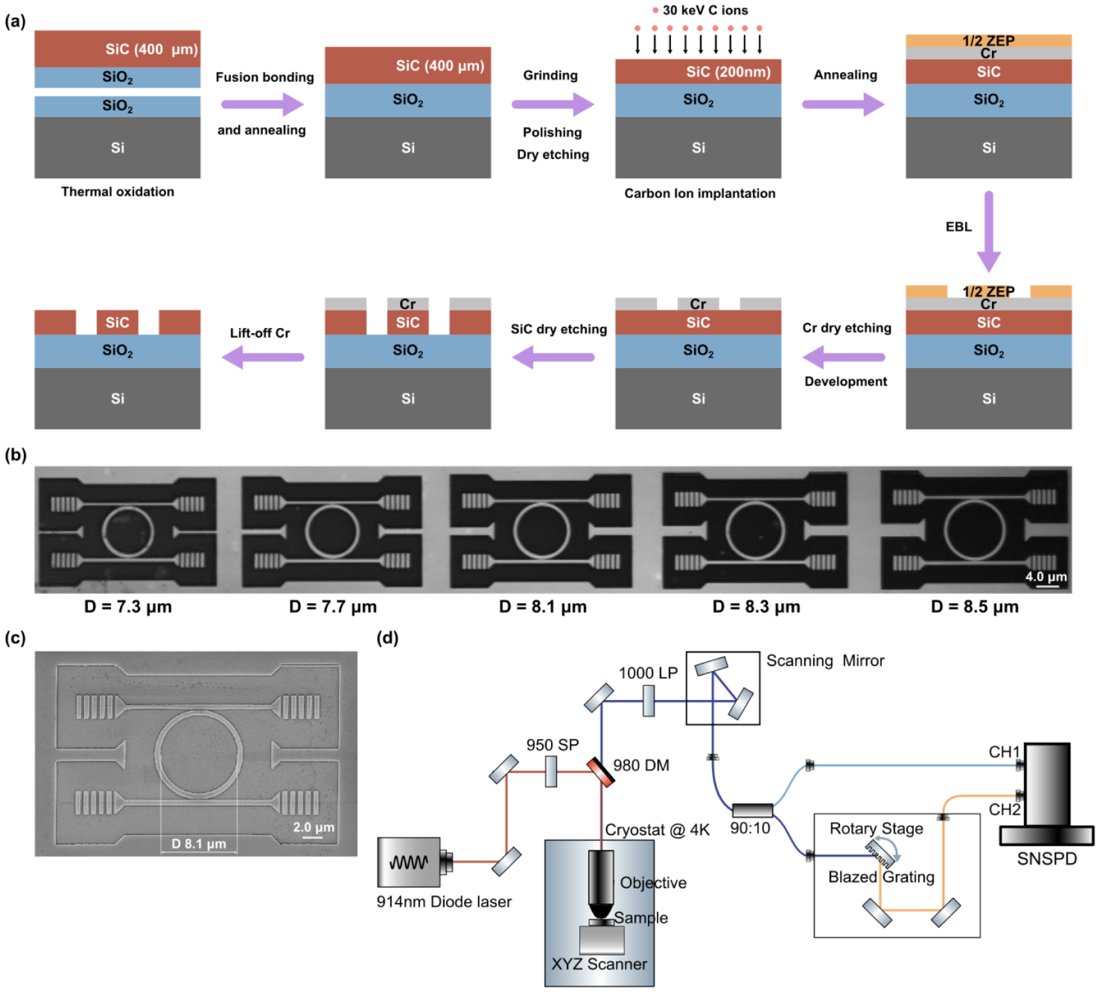

Figure 1. PL4 divacancy spins integrated microring cavities on 4H-SiCOI. (a) A 4H-SiC wafer with an epitaxial layer and a Si wafer were oxidized to form a thin layer of SiO_2 on the surface. The two wafers were then fusion-bonded through annealing to enhance the bonding strength. The 400 μm thick SiC membrane was thinned to a target thickness of 200 nm through successive grinding, mechanical polishing, and ICP dry etching. Divacancy spins were introduced into the membrane via carbon ion implantation followed by high-vacuum annealing. The fabrication of photonic devices began with the deposition of a 30 nm Cr layer onto the SiCOI substrate containing the ensemble spins. Microring cavities of varying diameters were patterned onto an electron beam resist (ZEP 520A) using electron beam lithography (EBL). After the resist was developed, a Cr mask was created through ICP dry etching, which was used to etch the designed photonic devices into the SiC substrate. Finally, the Cr mask was lifted off, and the devices were fabricated. (b) Optical image of fabricated miro-ring cavities with different diameters from 7.3 μm to 8.5 μm. (c) Scanning electron microscopy (SEM) image of the microring cavity with a diameter of 8.1 μm. (d) Optical setups used for device characterization. A custom-built 4K microscopy system collects the fluorescence from PL4 divacancy spins. The emission is directed to a 90:10 beam splitter for either optically detected magnetic resonance (ODMR) and spin control (10%, CH1 of SNSPD) or PL spectrum and lifetime measurements (90%). A blazed grating with a rotary stage is used in the PL spectrum measurements.

RESULTS

PL4 Divacancy Spins on 4H-SiCOI. Silicon carbide (SiC) divacancies are specific point defects in the SiC crystal lattice, formed by the absence of a silicon atom and an adjacent carbon atom.[32,33] These divacancies exhibit excellent optical and spin properties, making them highly promising for quantum technology applications.[34] The labels PL1−PL7 correspond to distinct defect types associated with various configurations of these divacancies in the 4H-SiC polytype.[33,35] Among these, the PL4 defect is particularly interesting, as it frequently appears as the most prominent peak in divacancy-related photoluminescence (PL) spectra generated via carbon ion implantation.[36] This prominence suggests that the PL4 configuration is more readily formed during fabrication.

To mitigate the adverse effects of ion irradiation on the spin properties, the SiCOI wafer employs a thinning and polishing technique[12] rather than the conventional smart-cut method.[10] As illustrated in Figure 1a, a 4H-SiC wafer with an epitaxial and thin SiO_2 layer is bonded to an oxidized Si wafer. The bonded SiC layer undergoes mechanical grinding followed by chemical-mechanical polishing (CMP) to achieve a thickness of several micrometers. A SiCOI wafer with a designed thickness of 200 nm is obtained after dry etching the SiC layer. Divacancy spins are generated in the SiC membrane via carbon ion implantation. The implantation was performed using 30 keV ions at a dose of 1.0×10^{13} cm^{-2}. This was followed by annealing in a high vacuum at 900 °C for 30 min to repair any remaining lattice damage. The fabrication of photonic devices began with the deposition of a 30 nm Cr layer on the SiCOI membrane. The microring cavities with different diameters were then patterned onto an electron beam resist (ZEP 520A) using an electron beam lithography overlay technique. After

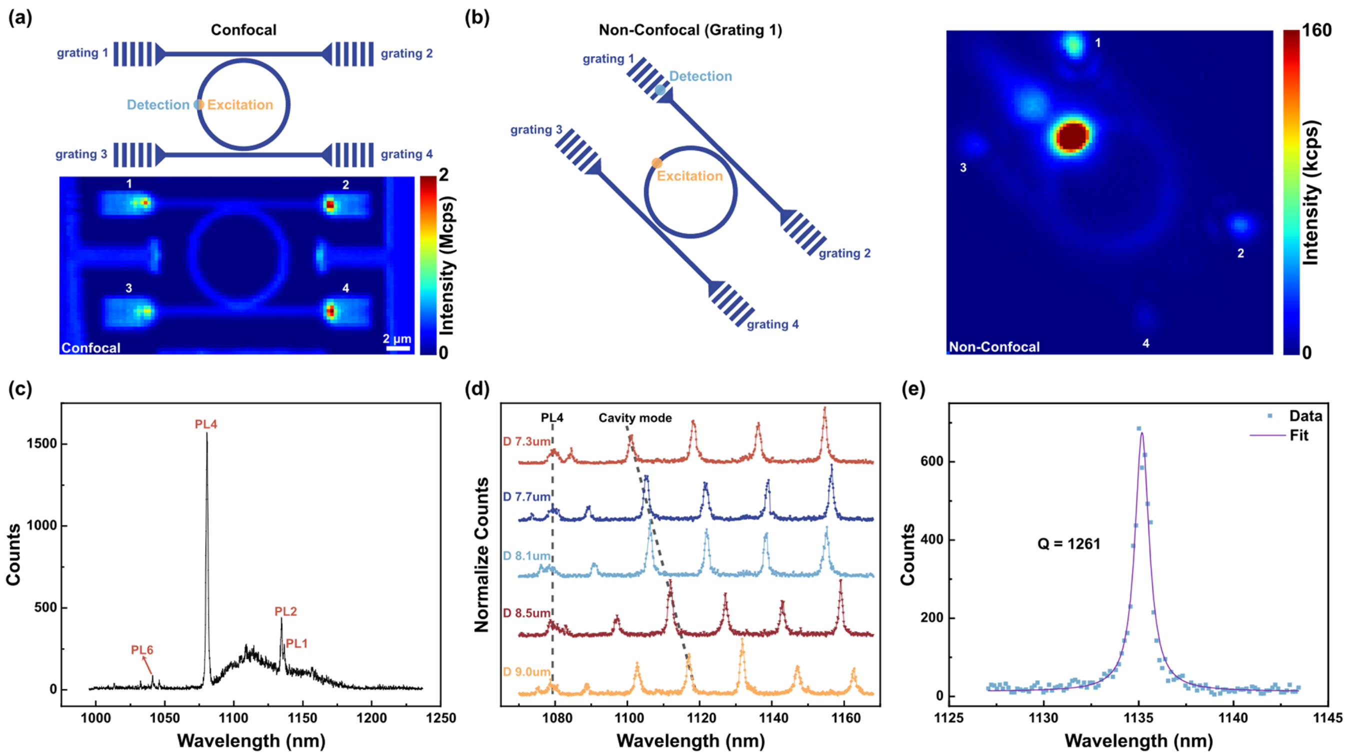

Figure 2. Optical characterization of the microring cavities at 4K. (a) The confocal scan map of the microring cavity at 4K shows that the microring and coupling waveguides, equipped with four grating couplers, align precisely with the designed geometry. (b) To collect the emission from the grating coupler 1, the excitation spot is maintained at the ring while the collection angle is varied using a scanning mirror in the collection arm. Four distinct emission spots from the grating couplers are clearly visible and marked, confirming that the divacancy PL can be coupled to the waveguide and emitted from the side grating couplers. (c). The full spectrum of divacancy PL at 0.2 mW excitation power and 4K is shown. The dominant peak is the zero-phonon line (ZPL) from PL4, while ZPLs from PL1, PL2, and PL6 are also observable, though with much lower intensity. (d). The PL spectrum acquired from grating 1 in Figure B shows different microring cavities with varying diameters under 0.4 mW excitation power. Multiple cavity modes are visible in the phonon sidebands with a free-spectral range (FSR) 14.8 ± 0.07 nm to 17.2 ± 0.02 nm. By altering the diameters, the cavity modes exhibit progressive wavelength shifts, as indicated by the dashed line. The ZPL from PL4 remains unchanged and weak, denoted by a dashed line, indicating it is not coupled with the cavity modes. (e). The measured cavity mode coupled with PL4 luminescence shows a quality factor (Q) of 1261 ± 39. A Lorentzian fit to the raw data is displayed in red.

developing the resist, the Cr mask was created through ICP dry etching. The photonic devices were fabricated by etching the SiC membrane with the patterned Cr as a hard mask.

After the Cr liftoff, the optical images of the fabricated microring cavities with diameters ranging from 7.3 μm to 8.5 μm are displayed in Figure 1b (refer to Figures S4 and S5 for the device design and simulation details and Figure S6 for PL4 polarization). The top-view scanning electron microscope (SEM) images of the microring cavities with a diameter of 8.1 μm are displayed in Figure 1c. The fabricated device's dimensions closely align with our design specifications. As depicted in Figure 1d, the fabricated microring cavities were characterized using a home-built confocal microscope system operating at 4K. A 914 nm diode laser was used to excite the vacancy spins. The fluorescence was then collected and detected with a superconducting nanowire single-photon detector (SNSPD). Based on the total emission rate, we estimate the concentration of the PL4 centers to be 5×10^{14} centers/cm^2. The emission is guided to a 90:10 fiber beam splitter either for spectrum and lifetime measurements (90%, channel 1) or for ODMR measurements (10%, channel 2), respectively. A blazed grating (600/mm) with a rotational state was utilized in the PL measurement and ZPL filtering. The dependence of the angle and wavelength was precharacterized by a tunable diode laser with a wavemeter.

Optical Characterization of the Microring Cavities at 4K. Optical characterization at 4K reveals detailed insights into the device's performance, as illustrated in Figure 2. Figure 2a displays the confocal scan map of the microring cavity, highlighting two coupling waveguides and four grating couplers that align with the designed geometry. By maintaining excitation within the microring and adjusting the collection angle using a scanning mirror, we captured the angle-dependent scan map, as depicted in Figure 2b. This scan map clearly shows four emission spots from each grating coupler, confirming the successful coupling of divacancy photoluminescence (PL) from the ring to the waveguide and side grating couplers. In addition to excitation at the ring, we also conducted PL spectrum measurements through excitation at the waveguide, as detailed in Figure S3. To confirm the effective coupling between the spin defects and the micro-cavity, we measured the PL spectrum collected from both the confocal spot and grating 1. The full spectrum of divacancy color centers under 0.2 mW confocal excitation is depicted in Figure 2c. The spectrum is dominated by the zero-phonon line (ZPL) from PL4, with additional ZPLs from PL1, PL2, and PL6 at much lower intensities.[33] The PL spectrum in Figure 2d was obtained from grating 1 under specific power excitation at the side of the microring. The spectra clearly show multiple cavity modes within the emission band of the PL4 divacancy

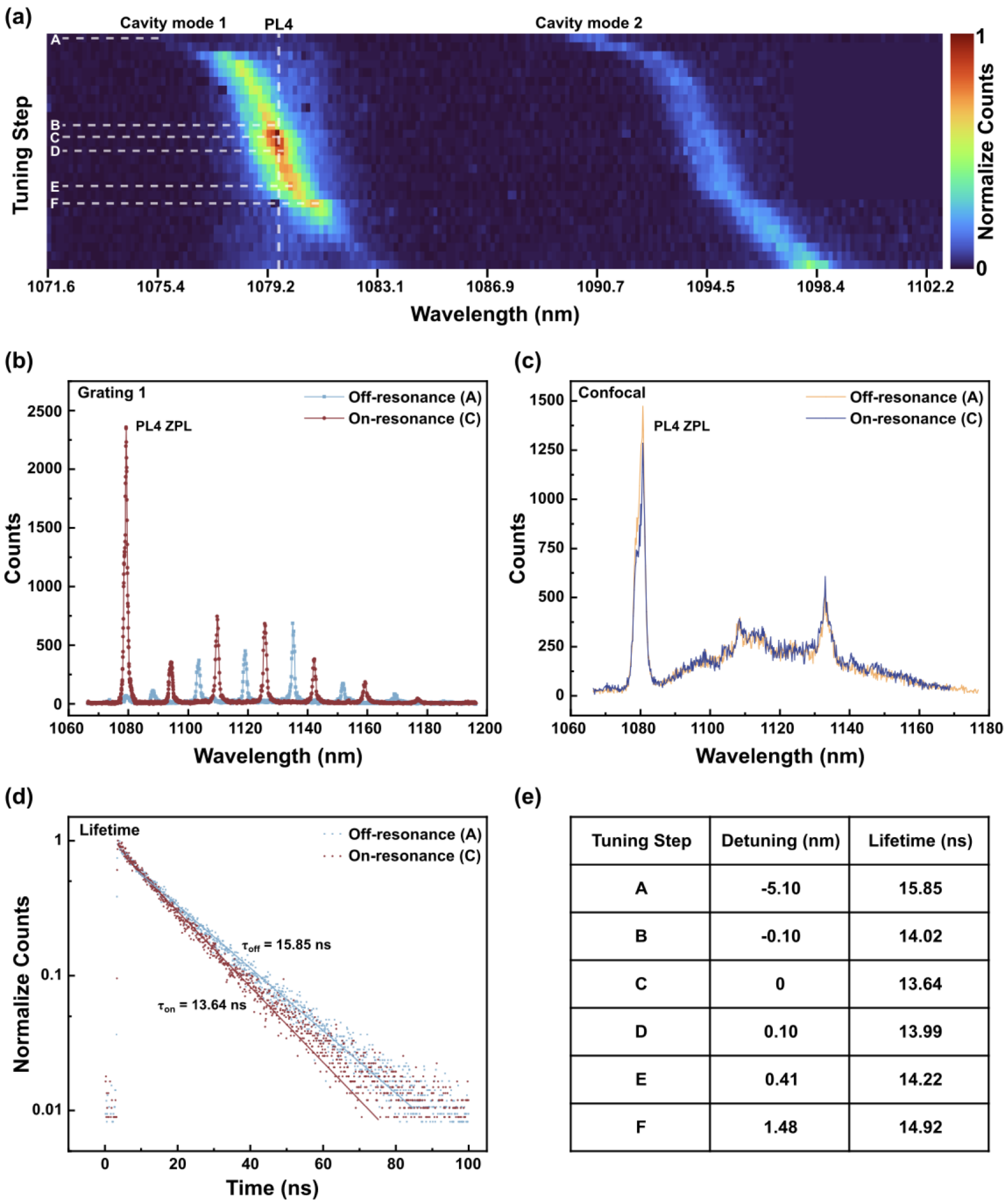

Tuning Step	Detuning (nm)	Lifetime (ns)
A	-5.10	15.85
B	-0.10	14.02
C	0	13.64
D	0.10	13.99
E	0.41	14.22
F	1.48	14.92

Figure 3. Continuous cavity mode tuning via gas condensation. (a). The intensity map shows the redshift of the cavity mode as nitrogen gas is continuously injected, causing the cavity mode to intersect the fixed ZPL of PL4 and resulting in significant emission enhancement. Points A−F represent specific stages within the continuous gas condensation process. (b) PL spectrum comparison between off-resonance (point A) and on-resonance (point D) under 0.2 mW excitation shows a 36-fold increase in ZPL intensity. (c) Confocal PL spectra for on- and off-resonance conditions show similar intensity, confirming that the emission enhancement is well confined within the cavity and the waveguide, finally emitted from the output grating coupler. (d) Lifetime measurements of the ZPL fitted with a single exponential function, indicating a reduction in lifetime from 15.85 ± 0.09 ns off-resonance to 13.64 ± 0.07 ns on-resonance. (e) Summary of lifetimes at points A−F, demonstrating that the closer the cavity mode is to the ZPL, the more pronounced the reduction in lifetime.

spin. Different colors represent microring cavities with varying diameters ranging from 7.3 to 8.9 μm, with free spectral range (FSR) from 14.8 ± 0.07 nm to 17.2 ± 0.02 nm. As the diameter changes, the shifts in the optical modes can be observed, as indicated by the dashed line. This shift demonstrates the coarse tunability (13 nm in total) of optical modes by altering the ring's predesigned dimensions. However, the zero-phonon line (ZPL) from PL4 is weak and also marked with a dashed line, indicating it is not effectively coupled with the existing modes. As displayed in Figure 2e, the measured cavity mode coupled with PL4 PL shows a quality factor Q of 1261 ± 39. The quality factors of the other microring resonators with diameters of 7.3 μm, 7.7 μm, 8.5 μm, and 8.9 μm were measured to be 1188 ± 55, 1218 ± 72, 1181 ± 88, and 943 ± 33, respectively. The relatively low Q factor is likely due to surface roughness, a consequence of imperfections in the etching process, which is visible in the rough sidewalls of the microring (as shown in Figure S8). These rough surface

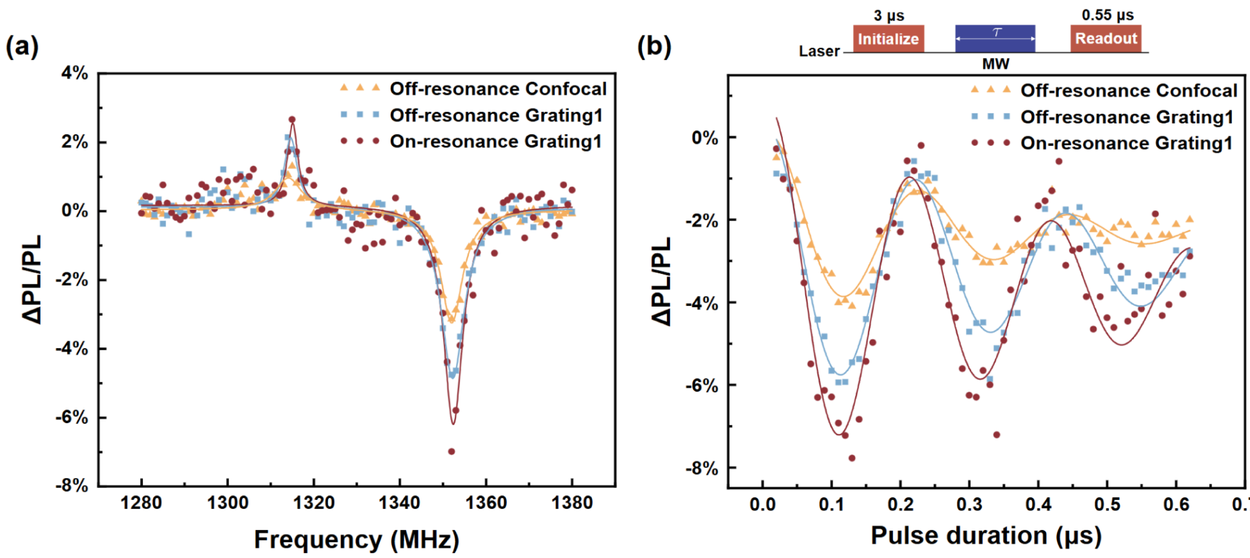

Figure 4. ODMR and coherent control of the PL4 spin in microring cavities. (a) Three ODMR measurements were obtained in (i) off-resonance from confocal scan, (ii) off-resonance from grating 1, and (iii) on-resonance from grating 1. All spectra reveal two peaks at 1315.1 ± 0.3 MHz and 1352.4 ± 0.2 MHz. From Lorentzian fitting, the ODMR contrast is extracted to be 3.2%, 4.8%, and 6.2%, respectively. On-resonance from the grating 1 case showed a 2-fold enhancement in ODMR contrast, highlighting the significant contribution of the ZPL filtering and boosting effect of the microcavity. (b) Rabi oscillations of the PL4 divacancy spin, demonstrating coherent control of PL4 spins both coupled and uncoupled with the microring cavity, in alignment with the observed ODMR contrast. The laser and microwave pulse sequences utilized for measuring the Rabi oscillations are illustrated.

conditions cause substantial scattering and absorption losses as light propagates through the cavity.[37] The observed sidewall roughness may result from several factors, including the micromasking effect[38] introduced by the etching of the metal hard mask, the balance between carbon residue and polymer deposition, and the small mode volume of the microring cavities, which makes them more sensitive to imperfections. To improve the Q factor, potential optimization avenues include using alternative mask materials (e.g., HSQ), refining plasma chemistry to reduce roughness. These approaches aim to reduce sidewall defects, minimize loss mechanisms, and enhance the overall performance of the resonators. Besides characterization at 4K, we also conducted room-temperature measurements of the fabricated microring cavities, summarized in Figure S1. Similar cavity modes can also be observed.

Continuous Cavity Mode Tuning via Gas Condensation. After conducting the initial optical characterization and confirming the coupling between the spin defects and the cavity, the tuning of the cavity mode and the strong enhancement of the zero-phonon line (ZPL) of PL4 within the cavity were demonstrated. A cavity with an 8.1 μm diameter was selected, whose optical mode is slightly blue-shifted compared to the ZPL wavelength. The optical mode can be gradually red-shifted using nitrogen gas condensation.[39] Figure 3a displays an intensity map showing the interaction between the cavity mode and the ZPL of PL4 as a function of gas injection steps. The cavity mode undergoes red shifting while the ZPL wavelength remains constant. A significant enhancement in emission is observed when the two intersect on the map. To facilitate the explanation of subsequent lifetime and PL spectrum measurements, seven points (A–F) are marked throughout the process. During the first three cycles, approximately 0.05 L of nitrogen gas at a pressure of 100 Pa was introduced into the cryostat per cycle. From that point until point F, the same volume of nitrogen gas (0.05 L) was introduced per cycle, but at a reduced pressure of 15 Pa. After point F, the introduction pressure was adjusted to 50 Pa while maintaining the same volume per cycle. This tuning process is reversible, and the system can return to its pretuned state simply by increasing the temperature. To further demonstrate the versatility of this tuning method, we applied it to modulate the cavity modes of another microring resonator with a diameter of 7.7 μm, as shown in Figure S7.

Figure 3b illustrates the PL spectrum at point A (off-resonance) and point D (on-resonance). The ZPL intensity experiences a 36-fold increase, with other modes showing no significant variation. This enhancement occurs only at the output coupler, as evidenced by the two similar confocal PL spectra measurements between on- and off-resonance shown in Figure 3c. This suggests that the enhanced coherent photons were effectively confined within the coupled waveguide. Lifetime measurements were performed using a 940 nm picosecond laser with a repetition rate of 10 MHz. As shown in Figure 3d, the temporal profile of the PL emission was fitted by a single exponential function, indicating a reduction in the lifetime from 15.85 ± 0.09 ns in the off-resonance case to 13.64 ± 0.07 ns when resonant with the cavity mode.

Next, we analyze the Purcell effect observed in our experiment. When the cavity mode is off-resonance, the total emission rate of uncoupled color centers is given by[17]

$$\frac{1}{\tau_{\text{off}}} = \frac{1}{\tau_{\text{ZPL}}} + \frac{1}{\tau_{\text{PSB}}}$$

where $1/\tau_{\text{ZPL}}$ and $1/\tau_{\text{PSB}}$ are the emission rates into ZPL and phonon sideband (PSB), respectively. When the cavity mode is on-resonance, the emission rate is modified as[17]

$$\frac{1}{\tau_{\text{on}}} = \frac{F+1}{\tau_{\text{ZPL}}} + \frac{1}{\tau_{\text{PSB}}}$$

where F is the Purcell factor, which can be estimated from the measured lifetimes using the relation:

https://doi.org/10.1021/acsphotonics.4c02574
ACS Photonics 2025, 12, 2988–2996

$$F = \frac{1}{\xi_{ZPL}}\left(\frac{\tau_{off}}{\tau_{on}} - 1\right)$$

where the ratio $\xi_{ZPL} = \tau_{off}/\tau_{ZPL}$ is equivalent to the branching ratio into the ZPL (Debye−Waller factor, DWF). The DWF was measured to be 0.031 based on the integration of the measured PL spectrum in Figure 2c. This DWF is consistent with the theoretically calculated value of 0.038,[40] corresponding to a Purcell factor of 5.23.

In the above calculation, we assume that $1/\tau_{off}$ is equal to the lifetime of centers in the unpatterned SiC membrane $1/\tau_0$. However, due to the presence of the photonic band gap, the optical density of the state is reduced, typically resulting in τ_{off} being generally slightly greater than τ_0.[15,41] The Purcell factor can also be estimated using the following relation:[15]

$$\mathrm{F} = \frac{\tau_0}{\mathrm{DWF}}\left(\frac{1}{\tau_{on}} - \frac{1}{\tau_{off}}\right)$$

where DWF is the Debye−Waller factor. τ_0 is measured to be 14.94 ± 0.08 ns (Figure S2 in the Supplementary Note 2), corresponding to a Purcell factor of 4.9. The lifetimes of various points of the whole gas condensation process from Figure 3a are summarized in Figure 3e. As anticipated, the closer the cavity mode is to the ZPL position, the more significant the reduction in lifetime.

ODMR and Coherent Control of the PL4 Spins in Microring Cavities. Optically detected magnetic resonance (ODMR) establishes a crucial interface between quantum spin systems and optical measurement, where microwave-driven spin transitions are converted into measurable photoluminescence changes.[42] This technique underpins defect-based quantum technologies, such as quantum sensing[43] and networks.[23,44] Therefore, ODMR contrast is a vital parameter that has gained significant attention. However, generating specific defect types among ensemble divacancy spins via implantation to increase ODMR contrast is extremely challenging because all polytopes may form. In on-chip sensing, the on-resonance enhancement of the specific ZPL serves as a filtering mechanism and increases the ODMR signal amplitude.[25] To perform spin-dependent measurements on defects within the cavity structure, a 20 μm copper wire is used as a microwave antenna near the device in the cryostation.

The PL4 defect is oriented along the basal planes, resulting in lower C_{1h} symmetry and nondegenerate spin transitions at zero magnetic fields ($B = 0$). Figure 4a presents the zero-field ODMR measurements obtained from both confocal detection and grating 1. The spectrum reveals two prominent peaks at 1315.1 ± 0.3 MHz and 1352.4 ± 0.2 MHz, which align with the reported values of 1.316 and 1.353 GHz in the literature.[33] The ODMR contrast improves by a factor of 2 when the PL emission is collected via the grating (on resonance) instead of confocally (off-resonance). This enhancement demonstrates that the microring cavity functions as a filter, increasing the proportion of PL4 photons in the total collected emission. Finally, the coherent control of PL4 spins both with and without coupling to the microring cavity has been performed. Figure 4b shows the Rabi oscillations of the PL4 divacancy spin, the contrast of Rabi rotation is consistent with the ODMR measurements.

CONCLUSION

In conclusion, we have successfully demonstrated the integration and control of spin defects in tunable microring cavities within thin-film 4H-SiC nanophotonics. By leveraging the cavity's resonance enhancement, a substantial 36-fold increase in zero-phonon line (ZPL) intensity was achieved, along with a 2-fold increase in optically detected magnetic resonance (ODMR) contrast compared to the off-resonance conditions. Coherent control of the microring cavity integrated PL4 spins was realized, highlighting the potential for integrating such systems into more complex quantum photonic circuits. While the N_2 gas method has limitations in nonlocal tuning, integrated microheaters offer a solution for nanoscale-localized thermal control within the 4H-SiCOI platform.[45] Our work provides important insights into defect-cavity interactions, paving the way for developing advanced silicon carbide-based quantum photonic devices with enhanced functionalities.

METHODS

4H-SiCOI and Microring Cavity Fabrication. Following the standard RCA cleaning process, a 4-in. 4H-SiC wafer with an epitaxial layer was prepared, featuring N-doping concentrations of 1×10^{18} cm^{-3} for the wafer and 5×10^{14} cm^{-3} for the epi-layer. The wafer and an oxidized silicon substrate were activated using 100 W O_2 plasma for 30 s. The two wafers were bonded together at room temperature under a pressure of 3000 N. To strengthen the bond, the structure was annealed at 800 °C for 6 h before proceeding to the grinding stage. The grinding process was conducted in two phases: initially, a 10 μm diamond slurry was used to grind the bonded wafer under a pressure of 600 N for around 10 h, reducing the SiC layer to approximately 30 μm. Subsequently, the SiC layer was further ground down to 10 μm using a 3 μm diamond slurry. A chemical mechanical polishing (CMP) process was then employed to eliminate any surface damage caused by the grinding. The SiCOI wafer was diced into individual dies, with each die undergoing ICP dry etching to achieve the final thickness (200 nm). This etching was performed using 100 W RF and 1000 W ICP power at 10 mTorr. To introduce ensemble divacancy spins, we performed ion implantation using 30 keV carbon ions with a dose of 1.0×10^{13} cm^{-2}. This was followed by annealing in a high vacuum at 900 °C for 30 min to repair any remaining lattice damage.

The fabrication of photonic devices began with the deposition of a 30 nm chromium (Cr) layer on a silicon-carbide-on-insulator (SiCOI) membrane. Microring cavities of varying diameters were then patterned onto an electron beam resist (ZEP 520A) using electron-beam lithography with an overlay technique. After resist development, the Cr hard mask was formed via inductively coupled plasma (ICP) dry etching. Specifically, the Cr etching process used an SF_6:O_2 gas mixture at a 1:100 ratio, achieving an etch rate of 400 nm/min under a chamber pressure of 6 mTorr and a substrate temperature stabilized at 20 °C. Following the formation of the Cr mask, the underlying SiC membrane was etched to define the photonic devices, guided by the patterned Cr hard mask. For the SiC etching step, the ICP system utilized an SF_6:O_2 gas mixture at a ratio of 20:1, resulting in a controlled etch rate of 100 nm/min. The RF power was set to 100 W, with the ICP power at 1000 W, operating at a chamber pressure of 10 mTorr.

https://doi.org/10.1021/acsphotonics.4c02574
ACS Photonics 2025, 12, 2988−2996

Device Characterization and Spin Control of Ensemble Spins. The fabricated microring cavities were characterized using a home-built confocal microscope operating at a temperature of 5 K within a Montana Cryostation closed-cycle cryostat (CryoAdvance 50). A near-infrared objective (Olympus, LCPLN50XIR) with a numerical aperture of 0.65 was employed, along with a single-mode fiber-coupled superconducting nanowire single-photon detector (PHOTEC). A 914 nm diode laser (MIL-III-914−300 mW) was used to excite the PL4 divacancy spins, while a 50 μm copper wire served as the microwave antenna above the device. All experimental sequences were synchronized using a pulse blaster (Spincore, PBESR-PRO-500-PCI). In lifetime measurements, a picosecond 940 nm laser (NKT Photonics, PIL1-094-40FC) and a time-correlated single-photon counting system (ID1000) were utilized.

■ ASSOCIATED CONTENT

Supporting Information

The Supporting Information is available free of charge at https://pubs.acs.org/doi/10.1021/acsphotonics.4c02574.

> Optical characterization of the devices at room temperature, lifetime measurement of the PL4 in the membrane and PL spectrum via waveguide excitation at 4K, simulation of micro-ring cavities, polarization of ZPL of PL4, continuous tuning of cavity modes within additional microring resonators (PDF)

■ AUTHOR INFORMATION

Corresponding Authors

Yu Zhou − *Ministry of Industry and Information Technology Key Lab of Micro-Nano Optoelectronic Information System, Guangdong Provincial Key Laboratory of Semiconductor Optoelectronic Materials and Intelligent Photonic Systems, Harbin Institute of Technology, Shenzhen 518055, PR China; Quantum Science Center of Guangdong-HongKong-Macao Greater Bay Area (Guangdong), Shenzhen 518045, PR China;* orcid.org/0000-0002-9810-5307; Email: zhouyu2022@hit.edu.cn

Xin Ou − *State Key Laboratory of Materials for Integrated Circuits, Shanghai Institute of Microsystem and Information Technology, Chinese Academy of Sciences, Shanghai 200050, PR China; The Center of Materials Science and Optoelectronics Engineering, University of Chinese Academy of Sciences, Beijing 100049, PR China;* orcid.org/0000-0002-0316-9958; Email: ouxin@mail.sim.ac.cn

Qinghai Song − *Ministry of Industry and Information Technology Key Lab of Micro-Nano Optoelectronic Information System, Guangdong Provincial Key Laboratory of Semiconductor Optoelectronic Materials and Intelligent Photonic Systems, Harbin Institute of Technology, Shenzhen 518055, PR China; Pengcheng Laboratory, Shenzhen 518055, PR China; Quantum Science Center of Guangdong-HongKong-Macao Greater Bay Area (Guangdong), Shenzhen 518045, PR China; Collaborative Innovation Center of Extreme Optics, Shanxi University, Taiyuan 030006 Shanxi, PR China;* orcid.org/0000-0003-1048-411X; Email: qinghai.song@hit.edu.cn

Authors

Tongyuan Bao − *Ministry of Industry and Information Technology Key Lab of Micro-Nano Optoelectronic Information System, Guangdong Provincial Key Laboratory of Semiconductor Optoelectronic Materials and Intelligent Photonic Systems, Harbin Institute of Technology, Shenzhen 518055, PR China*

Qi Luo − *Ministry of Industry and Information Technology Key Lab of Micro-Nano Optoelectronic Information System, Guangdong Provincial Key Laboratory of Semiconductor Optoelectronic Materials and Intelligent Photonic Systems, Harbin Institute of Technology, Shenzhen 518055, PR China*

Ailun Yi − *State Key Laboratory of Materials for Integrated Circuits, Shanghai Institute of Microsystem and Information Technology, Chinese Academy of Sciences, Shanghai 200050, PR China; The Center of Materials Science and Optoelectronics Engineering, University of Chinese Academy of Sciences, Beijing 100049, PR China*

Bo Liang − *Ministry of Industry and Information Technology Key Lab of Micro-Nano Optoelectronic Information System, Guangdong Provincial Key Laboratory of Semiconductor Optoelectronic Materials and Intelligent Photonic Systems, Harbin Institute of Technology, Shenzhen 518055, PR China*

Yao Zhang − *Ministry of Industry and Information Technology Key Lab of Micro-Nano Optoelectronic Information System, Guangdong Provincial Key Laboratory of Semiconductor Optoelectronic Materials and Intelligent Photonic Systems, Harbin Institute of Technology, Shenzhen 518055, PR China*

Hai-Bo Hu − *Ministry of Industry and Information Technology Key Lab of Micro-Nano Optoelectronic Information System, Guangdong Provincial Key Laboratory of Semiconductor Optoelectronic Materials and Intelligent Photonic Systems, Harbin Institute of Technology, Shenzhen 518055, PR China; Pengcheng Laboratory, Shenzhen 518055, PR China*

Shen Lai − *Institute of Applied Physics and Materials Engineering, Faculty of Science and Technology, University of Macau, Macau 999078, PR China;* orcid.org/0000-0001-7641-972X

Zhengtong Liu − *Pengcheng Laboratory, Shenzhen 518055, PR China*

Shumin Xiao − *Ministry of Industry and Information Technology Key Lab of Micro-Nano Optoelectronic Information System, Guangdong Provincial Key Laboratory of Semiconductor Optoelectronic Materials and Intelligent Photonic Systems, Harbin Institute of Technology, Shenzhen 518055, PR China; Pengcheng Laboratory, Shenzhen 518055, PR China; Quantum Science Center of Guangdong-HongKong-Macao Greater Bay Area (Guangdong), Shenzhen 518045, PR China; Collaborative Innovation Center of Extreme Optics, Shanxi University, Taiyuan 030006 Shanxi, PR China;* orcid.org/0000-0002-0751-9556

Complete contact information is available at: https://pubs.acs.org/10.1021/acsphotonics.4c02574

Author Contributions

○T.B., Q.L., and A.Y. contributed equally.

Funding

We acknowledge the support from the Innovation Program for Quantum Science and Technology (No. 2024ZD0302100), the National Key R&D Program of China (grant no. 2021YFA1400802, 2022YFA1404601, 2023YFB2806700), the National Natural Science Foundation of China (grant no. 12304568, 11934012, 62293520, 62293522, 62293521, 12074400, and 62205363), the GuangDong Basic and Applied Basic Research Foundation (grant no. 2022A1515110382), Shenzhen Fundamental research project (grant no. JCYJ20241202123903005, JCYJ20230807094408018), the Guangdong Provincial Quantum Science Strategic Initiative (GDZX2403004, 2406002, 2303001, 2306002, 2200001), the Young Elite Scientists Sponsorship Program by CAST, New Cornerstone Science Foundation through the XPLORER PRIZE, Shanghai Science and Technology Innovation Action Plan Program (grant no. 22JC1403300), the CAS Project for Young Scientists in Basic Research (grant no. YSBR-69), the Major Key Project of PCL, and the Talent Program of Guangdong Province (grant no. 2021CX02X465).

Notes

The authors declare no competing financial interest.

■ REFERENCES

(1) Anderson, C. P.; Glen, E. O.; Zeledon, C.; Bourassa, A.; Jin, Y.; Zhu, Y.; Vorwerk, C.; Crook, A. L.; Abe, H.; Ul-Hassan, J.; Ohshima, T. Five-second coherence of a single spin with single-shot readout in silicon carbide. *Sci. Adv.* **2022**, *8* (5), No. eabm5912.

(2) Miao, K. C. Universal coherence protection in a solid-state spin qubit. *Science* **2020**, *369*, 1493−1497.

(3) Anderson, C. P. Electrical and optical control of single spins integrated in scalable semiconductor devices. *Science* **2019**, *366*, 1225−1230.

(4) Falk, A. L. Electrically and mechanically tunable electron spins in silicon carbide color centers. *Phys. Rev. Lett.* **2014**, *112*, 187601.

(5) Hu, H.; Zhou, Y.; Yi, A.; Bao, T.; Liu, C.; Luo, Q.; Zhang, Y.; Wang, Z.; Li, Q.; Lu, D. Room-temperature waveguide integrated quantum register in a semiconductor photonic platform. *Nat. Commun.* **2024**, *15* (1), 10256.

(6) Klimov, P. V.; Falk, A.; Buckley, B. B.; Awschalom, D. D. Electrically driven spin resonance in silicon carbide color centers. *Phys. Rev. Lett.* **2014**, *112*, 8, .

(7) Lai, X. Y. Single-Shot Readout of a Nuclear Spin in Silicon Carbide. *Phys. Rev. Lett* **2024**, *132*, 180803.

(8) Niethammer, M.; Widmann, M.; Rendler, T.; Morioka, N.; Chen, Y.-C.; Stöhr, R.; Hassan, J. U.; Onoda, S.; Ohshima, T.; Lee, S.-Y.; Mukherjee, A. Coherent electrical readout of defect spins in silicon carbide by photo-ionization at ambient conditions. *Nat. Commun* **2019**, *10* (1), 5569.

(9) Lukin, D. M.; Guidry, M. A.; Vučković, J. Integrated quantum photonics with silicon carbide: Challenges and prospects. *PRX Quantum* **2020**, *1* (2), 20102.

(10) Castelletto, S. Silicon carbide photonics bridging quantum technology. *ACS Photonics* **2022**, *9*, 1434−1457.

(11) Yi, A.; Wang, C.; Zhou, L.; Zhu, Y.; Zhang, S.; You, T.; Zhang, J.; Ou, X. Silicon carbide for integrated photonics. *Appl. Phys. Rev* **2022**, *9* (3), 3.

(12) Lukin, D. M. 4H-silicon-carbide-on-insulator for integrated quantum and nonlinear photonics. *Nat. Photonics* **2020**, *14*, 330−334.

(13) Wang, X. D. Waveguide-coupled deterministic quantum light sources and post-growth engineering methods for integrated quantum photonics. *Chip* **2022**, *1*, 100018.

(14) Gadalla, M. N.; Greenspon, A. S.; Defo, R. K.; Zhang, X.; Hu, E. L. Enhanced cavity coupling to silicon vacancies in 4H silicon carbide using laser irradiation and thermal annealing. *Proc. Natl. Acad. Sci. U. S. A* **2021**, *118* (12), No. e2021768118.

(15) Bracher, D. O.; Zhang, X.; Hu, E. L. Selective Purcell enhancement of two closely linked zero-phonon transitions of a silicon carbide color center. *Proc. Natl. Acad. Sci. U. S. A* **2017**, *114*, 4060−4065.

(16) Fröch, J. E.; Li, C.; Chen, Y.; Toth, M.; Kianinia, M.; Kim, S. Purcell Enhancement of a Cavity-Coupled Emitter in Hexagonal Boron Nitride. *Small* **2022**, *18*, 2104805.

(17) Faraon, A.; Barclay, P. E.; Santori, C.; Fu, K. M. C.; Beausoleil, R. G. Resonant enhancement of the zero-phonon emission from a colour centre in a diamond cavity. *Nat. Photonics* **2011**, *5*, 301−305.

(18) Neumann, P. Single-shot readout of a single nuclear spin. *Science* **2010**, *329*, 542−544.

(19) Economou, S. E.; Dev, P. Spin-photon entanglement interfaces in silicon carbide defect centers. *Nanotechnology* **2016**, *27* (50), 504001.

(20) Gao, W. B.; Imamoglu, A.; Bernien, H.; Hanson, R. Coherent manipulation, measurement and entanglement of individual solid-state spins using optical fields. *Nat. Photonics* **2015**, *9*, 363−373.

(21) Kalb, N. Entanglement distillation between solid-state quantum network nodes. *Science* **2017**, *356*, 928−932.

(22) Stas, P.-J. Robust multi-qubit quantum network node with integrated error detection. *Science* **2022**, *378*, 557−560.

(23) Hermans, S. L. N. Qubit teleportation between non-neighbouring nodes in a quantum network. *Nature* **2022**, *605*, 663−668.

(24) Crook, A. L. Purcell enhancement of a single silicon carbide color center with coherent spin control. *Nano Lett* **2020**, *20*, 3427−3434.

(25) Calusine, G.; Politi, A.; Awschalom, D. D. Cavity-Enhanced Measurements of Defect Spins in Silicon Carbide. *Phys. Rev. Appl*, **2016**, *6*, 1, .

(26) Lukin, D. M.; Guidry, M. A.; Yang, J.; Ghezellou, M.; Deb Mishra, S.; Abe, H.; Ohshima, T.; Ul-Hassan, J.; Vučković, J. Two-emitter multimode cavity quantum electrodynamics in thin-film silicon carbide photonics. *Phys. Rev. X* **2023**, *13* (1), 11005.

(27) Lu, X.; McClung, A.; Srinivasan, K. High-Q slow light and its localization in a photonic crystal microring. *Nat. Photonics* **2022**, *16*, 66−71.

(28) Hodaei, H.; Miri, M. A.; Heinrich, M.; Christodoulides, D. N.; Khajavikhan, M. Parity-time-symmetric microring lasers. *Science* **2014**, *346*, 975−978.

(29) Zheng, Y.; Pu, M.; Ou, H.; Ou, X.; Yi, A. 4H-SiC microring resonators for nonlinear integrated photonics. *Opt. Lett* **2019**, *44* (23), 5784−5787.

(30) Gondarenko, A.; Levy, J. S.; Lipson, M. High confinement micron-scale silicon nitride high Q ring resonator. *Opt. Express* **2009**, *17*, 11366.

(31) Soref, R.; De Leonardis, F. Classical and quantum photonic sources based upon a nonlinear GaP/Si-superlattice micro-ring resonator. *Chip* **2022**, *1*, 100011.

(32) Son, N. T.; Carlsson, P.; Ul Hassan, J.; Janzén, E.; Umeda, T.; Isoya, J.; Gali, A.; Bockstedte, M.; Morishita, N.; Ohshima, T.; Itoh, H. Divacancy in 4h-sic. *Phys. Rev. Lett* **2006**, *96* (5), 55501.

(33) Falk, A. L.; Buckley, B. B.; Calusine, G.; Koehl, W. F.; Dobrovitski, V. V.; Politi, A.; Zorman, C. A.; Feng, P. X.-L.; Awschalom, D. D. Polytype control of spin qubits in silicon carbide. *Nat. Commun* **2013**, *4* (1), 1819.

(34) Koehl, W. F.; Buckley, B. B.; Heremans, F. J.; Calusine, G.; Awschalom, D. D. Room temperature coherent control of defect spin qubits in silicon carbide. *Nature* **2011**, *479*, 84−87.

(35) Ivády, V.; Davidsson, J.; Delegan, N.; Falk, A. L.; Klimov, P. V.; Whiteley, S. J.; Hruszkewycz, S. O.; Holt, M. V.; Heremans, F. J.; Son, N. T.; Awschalom, D. D. Stabilization of point-defect spin qubits by quantum wells. *Nat. Commun* **2019**, *10* (1), 5607.

(36) Wang, J.-F. Optical charge state manipulation of divacancy spins in silicon carbide under resonant excitation. *Photonics Res* **2021**, *9*, 1752.

(37) Wang, C.; Fang, Z.; Yi, A.; Yang, B.; Wang, Z.; Zhou, L.; Shen, C.; Zhu, Y.; Zhou, Y.; Bao, R.; Li, Z. High-Q microresonators on 4H-silicon-carbide-on-insulator platform for nonlinear photonics. *Light: sci. Appl* **2021**, *10* (1), 139.

(38) Racka-Szmidt, K.; Stonio, B.; Żelazko, J.; Filipiak, M.; Sochacki, M. A Review: Inductively Coupled Plasma Reactive Ion Etching of Silicon Carbide. *Materials 2022* **2022**, *15*, 123.

(39) Lee, J. C.; Bracher, D. O.; Cui, S.; Ohno, K.; McLellan, C. A.; Zhang, X.; Andrich, P.; Alemán, B.; Russell, K. J.; Magyar, A. P.;

Aharonovich, I. Deterministic coupling of delta-doped nitrogen vacancy centers to a nanobeam photonic crystal cavity. *Appl. Phys. Lett*, **2014**, *105*, 26, .
(40) Csóré, A.; Ivanov, I. G.; Son, N. T.; Gali, A. Fluorescence spectrum and charge state control of divacancy qubits via illumination at elevated temperatures in 4H silicon carbide. *Phys. Rev. B*, **2022**, *105*, 165108, .
(41) Faraon, A.; Santori, C.; Huang, Z.; Acosta, V. M.; Beausoleil, R. Coupling of nitrogen-vacancy centers to photonic crystal cavities in monocrystalline diamond. *Phys. Rev. Lett.* **2012**, *109* (3), 033604.
(42) Doherty, M. W. The nitrogen-vacancy colour centre in diamond. *Phys. Rep.* **2013**, *528*, 1−45.
(43) Du, J.; Shi, F.; Kong, X.; Jelezko, F.; Wrachtrup, J. Single-molecule scale magnetic resonance spectroscopy using quantum diamond sensors. *Rev. Mod. Phys.* **2024**, *96*, 025001.
(44) Awschalom, D. D.; Hanson, R.; Wrachtrup, J.; Zhou, B. B. Quantum technologies with optically interfaced solid-state spins. *Nat. Photonics* **2018**, *12*, 516−527.
(45) Zhu, Y.; Liu, R.; Yi, A.; Wang, X.; Qin, Y.; Zhao, Z.; Zhao, J.; Chen, B.; Zhang, X.; Song, S.; Huo, Y. A hybrid single quantum dot coupled cavity on a CMOS-compatible SiC photonic chip for Purcell-enhanced deterministic single-photon emission. *Light: sci. Appl.* **2025**, *14* (1), 1−11.

https://doi.org/10.1021/acsphotonics.4c02574
ACS Photonics 2025, 12, 2988−2996